

Review articles

Complementary aspects of diffusion imaging and fMRI; I: structure and function

Robert V. Mulkern^{a,b,*}, Peter E. Davis^c, Steven J. Haker^b, Raul San Jose Estepar^b,
Lawrence P. Panych^b, Stephan E. Maier^b, Michael J. Rivkin^c

^aDepartment of Radiology, Children's Hospital, Harvard Medical School, Boston, MA 02115, USA

^bDepartment of Radiology, Brigham and Women's Hospital, Harvard Medical School, Boston, MA 02115, USA

^cDepartments of Neurology, Radiology and Psychiatry, Children's Hospital, Harvard Medical School, Boston, MA 02115, USA

Received 2 December 2005; accepted 2 January 2006

Abstract

Studying the intersection of brain structure and function is an important aspect of modern neuroscience. The development of magnetic resonance imaging (MRI) over the last 25 years has provided new and powerful tools for the study of brain structure and function. Two tools in particular, diffusion imaging and functional MRI (fMRI), are playing increasingly important roles in elucidating the complementary aspects of brain structure and function. In this work, we review basic technical features of diffusion imaging and fMRI for studying the integrity of white matter structural components and for determining the location and extent of cortical activation in gray matter, respectively. We then review a growing body of literature in which the complementary aspects of diffusion imaging and fMRI, applied as separate examinations but analyzed in tandem, have been exploited to enhance our knowledge of brain structure and function.

© 2006 Elsevier Inc. All rights reserved.

Keywords: Diffusion imaging; Functional magnetic resonance imaging (fMRI); Structure; Function; Brain

1. Introduction

Within the context of clinical magnetic resonance imaging (MRI) of the brain, diffusion imaging and functional magnetic resonance imaging (fMRI) play relatively minor roles in comparison to conventional T1- and T2-weighted imaging methods. Diffusion-weighted imaging has been found useful for one very important application, the detection and evaluation of acute stroke [1–5], and may yet play a role in assessing the response of tumors to therapy [6,7]. The role of fMRI is less well established clinically but is of enormous interest to the many students of brain function and activity. The information contained in both diffusion imaging and fMRI studies is, however, unique and, in some sense, complementary. The most advanced diffusion imaging sequences gather information which can be processed into maps that reflect white matter fiber tract integrity and direction. Advanced processing of fMRI acquisitions can be

used to identify regions of the brain, primarily in gray matter, which demonstrate hemodynamic responses to specific tasks and make estimates of the degree of brain activation within those regions. In this work, we focus on brief descriptions of the basic methodologies and then review the available literature studies which have combined the complementary information of diffusion imaging and fMRI to study the relationship between structure and function. Areas covered include the primary visual and motor systems as well as studies involving brain disorders like multiple sclerosis or the effects of specific brain lesions. In a later work, we will review how diffusion weighting of the blood oxygenation level-dependent (BOLD) signal used for fMRI studies has been used to elucidate the physical and physiological mechanisms responsible for the BOLD signal, a separate type of study which also represents complementary aspects of diffusion imaging and fMRI.

2. Diffusion imaging

The physical principles and medical applications of diffusion imaging have been covered extensively in several

* Corresponding author. Department of Radiology, Children's Hospital, Harvard Medical School, Boston, MA, USA.

E-mail address: rmulkern@yahoo.com (R.V. Mulkern).

texts [8,9], so only a brief overview of the salient points is provided here. Generally speaking, diffusion imaging refers to sensitizing MRIs to the molecular motion of the water molecules being imaged. The basic methodology for sensitizing MR signals to molecular diffusion was introduced in the mid 60s by Stejskal and Tanner [10] who suggested placing a pair of balanced magnetic field gradients about the 180 refocusing pulse of a spin-echo acquisition. Different levels of gradient strength (g), duration (δ) and separation of the leading edges (Δ) of the two gradient pulses lead to different levels of spin echo signal attenuation due to the diffusive motions, as characterized by a molecular diffusion coefficient (D). The level of diffusion sensitivity is expressed through the so-called b factor given by

$$b = (g\gamma\delta)^2(\Delta - \delta/3) \quad (1)$$

where γ is the proton gyromagnetic ratio ($2\pi \times 4258$ Hz/gauss), and the spin echo signal is attenuated by the factor $\exp(-bD)$. The simplest measurement of the molecular diffusion coefficient D may be performed by acquiring two signals, S_0 and S_1 , with different b factors, b_0 and b_1 . The value of D may then be evaluated from the ratio of the two signal intensities via

$$D = (b_1 - b_0)^{-1} \ln(S_0/S_1) \quad (2)$$

where b_1 is the larger of the two b factors. Typically, b_0 is very small, on the order of 5 s/mm², while b_1 values are generally in the 750–1000-s/mm² range. The tissue diffusion coefficients are conveniently expressed in units of square micrometer per millisecond and typically range from 0.1 to 3 $\mu\text{m}^2/\text{ms}$.

The advent of modern MRI technology introduced in the early 80s proved highly adaptable to diffusion imaging. Spin echo imaging sequences using magnetic field gradients for signal localization were, and of course remain, commonplace imaging strategies. Le Bihan et al. [11] recognized the possibility of incorporating the classic Tanner–Stejskal pulsed gradient pair about the refocusing pulse within spin echo imaging sequences and succeeded in generating the first diffusion-weighted images of the human brain in the clinical setting. This basic approach is still employed today to generate diffusion-weighted images, although now, echo planar imaging (EPI) readouts are commonly used to hasten the imaging process [12].

Recognized early on was the fact that water diffusion in tissue was subject to many more motion pathways than, say, water molecules within a cup of tea. Restrictions to diffusion in the form of membranes and/or intracellular organelles as well as the more complex, tortuous pathways in capillary beds and small vessels associated with blood perfusion significantly increased the complexity of the diffusion process. As such, the simple exponential decay with increasing b factor and the independence of the measured diffusion coefficient on the so-called diffusion time, $\Delta - \delta/3$, contained within the b factor definition, are

not generally features of tissue water diffusion. Thus, the term *apparent diffusion coefficient* has been extensively used to describe tissue water diffusion. In respect for the meaning of the word *apparent*, we prefer not to use this term because, in our view, it could just as well be applied to other tissue contrast parameters associated with MRI like the transverse relaxation time T_2 . It must be appreciated, however, that any measurement of the tissue water diffusion coefficient D reflects a number of different contributions, and as such, the details of the acquisition pulse sequence can significantly influence the measured value of D . The most obvious example of this phenomenon, as quickly recognized by the imaging community [13,14], was the sensitivity of D to the direction of the diffusion sensitization gradients, a topic to which we now turn.

Myelinated fiber tracts constitute a major component of white matter in the mature brain and offer a preferred local direction for water molecules to travel, analogous to what water molecules might experience in the fibers of a stalk of celery. As a consequence, D , as measured with the diffusion sensitization gradients placed parallel to the fibers, is found to be larger than D measured with the gradients applied perpendicular to the fibers [13,14]. To allow for a measure of D , which can be reliably used as a “rotationally invariant” quantity — a quantity independent of the particular diffusion sensitization directions employed, the simple concept of a scalar value for D , appropriate for isotropic diffusion in simple liquids, must be abandoned in favor of the diffusion tensor generalization [15–18]. In this model, the diffusion process is characterized by a 3×3 symmetric matrix, the diffusion tensor, the six independent elements of which can only be evaluated by sampling at least six noncolinear diffusion sensitization directions. Though this tensor is a mathematical object with specific properties, a convenient conceptual representation of the tensor is that of an ellipsoid with three principal axes, one long axis and two shorter perpendicular axes, which may or may not be of equal length. The lengths and directions of the three axes are the eigenvalues and eigenvectors of the tensor, respectively, as calculated from diagonalization of the 3×3 diffusion tensor matrix. They represent the primary, secondary and tertiary modes of diffusion within a given voxel.

The simplest application of the diffusion tensor model involves measuring diffusion coefficients along three orthogonal directions. This approach yields sufficient information to obtain the sum of the diagonal elements of the matrix, known as the trace. This quantity is rotationally invariant, or independent of the three orthogonal directions used for its measurement and, so, provides a robust measure of a tissue-specific “average” diffusion coefficient D_{ave} given by

$$D_{\text{ave}} = (D_{\text{xx}} + D_{\text{yy}} + D_{\text{zz}})/3 \quad (3)$$

where D_{xx} , D_{yy} and D_{zz} are the diagonal elements of the diffusion tensor. The use of only three diffusion sensitization directions simplifies and shortens diffusion acquisitions

compared to full tensor acquisitions and is generally sufficient for the primary clinical application of diffusion imaging, which is the detection of acute stroke [1–5]. For studying the integrity and depicting the directionality of white matter tracts, however, additional information from the full diffusion tensor is generally sought by measuring diffusion coefficients from at least six diffusion sensitization directions, along with a baseline (b_0) sampling. Of course, this approach requires more scan time, but there are several rewards one may enjoy when estimates of all six diffusion tensor elements are measured. The most commonly reported among these is a rotationally invariant measure of the diffusion anisotropy, as embodied in the so-called fractional anisotropy (FA) parameter given by the following formula:

$$FA = \left[(\lambda_1 - \lambda_2)^2 + (\lambda_2 - \lambda_3)^2 + (\lambda_1 - \lambda_3)^2 \right]^{1/2} / [2(\lambda_1^2 + \lambda_2^2 + \lambda_3^2)]^{1/2} \quad (4)$$

where λ_1 , λ_2 and λ_3 are the eigenvalues of the diffusion tensor obtained using all six tensor elements including the off-diagonal elements D_{xy} , D_{xz} and D_{yz} . The FA value ranges from 0 to 1 and is a rotationally invariant measure of the degree of anisotropy associated with the diffusion of water molecules. For example, if a water molecule is equally likely to wander off in any given direction, as in our hypothetical cup of tea, then this is referred to as isotropic diffusion, and FA is 0. If, on the other hand, the water molecule is forced to wander along only one direction, as in a severely restricted microtubule, then the FA would be 1. Typical values for FA in mature white matter are in the 0.15–0.90 range and are generally thought to reflect, to some degree, the extent of myelination and the thickness of the axons, although even in unmyelinated fibers, anisotropic effects are observed [19–24].

In addition to the FA, the directions of the three eigenvectors — primary, secondary and tertiary — of the diffusion tensor are obtained for each voxel. These directions, primarily that of the primary eigenvector, are often mapped using vectorial displays although more complex color displays and/or maps of the tensor ellipsoids, which reflect characteristics of all three eigenvectors and their rank order, have also been suggested for displaying diffusion tensor information [16,25–27].

As diffusion tensor imaging (DTI) developed, so did an interest in proceeding beyond assessing the diffusion properties of individual voxels and towards generating information regarding intervoxel relationships from which one might infer and display actual white matter fiber tracts coursing through large regions of the brain. Thus, DTI's reckless daughter¹, diffusion tensor tractography (DTT), was born [28–35]. A number of approaches have been

introduced and demonstrated for performing DTT, and the field has matured considerably over the last several years, providing a powerful new tool for exploring brain connections. The basic idea behind DTT is to determine the most likely route that a water molecule would choose to enter or exit a voxel, as based on the primary preferred direction of diffusion within that voxel and its neighbors. One begins by selecting a starting or “seed” voxel and then begins the tracking algorithm. From each new voxel encountered, the process is repeated, allowing the daughter to wander along the path specified at each step by the primary direction of water diffusion, the presumed direction of the white matter fiber tracts. Simple in principle, computationally demanding in practice and fraught with danger associated with noise, vanishing anisotropies and strange voxels in which distinct fiber tracts may cross, the reckless daughter proceeds from voxel to voxel, leaving behind a colored trail outlining the fiber tract like a piece of spaghetti. Sprinkling the brain with different “seed points” allows for multiple paths to be formed throughout the brain and results in whole-brain tractographic maps.

Whether a mechanistic approach [28–31] or a probabilistic approach [32–35] to DTT is employed, basic thresholds must be selected by the operator when computing the fiber tracts. One threshold that must be considered is the FA parameter discussed above. For example, if a voxel is entered in which the FA value becomes quite low, then the tracking process has probably led to an area of grey matter or cerebrospinal fluid (CSF) and should stop. Another threshold parameter that must be considered in deciding which way to proceed from a given voxel is the angle between the primary eigenvector within that voxel and the equivalent vector in the neighboring voxels. The inner product (IP) of two primary eigenvectors in voxels i and j

$$IP = \lambda_{1i} \cdot \lambda_{1j} \quad (5)$$

is proportional to $\cos\theta$, where θ is the angular difference between the vectors and, thus, is often used to help determine the path followed by the intrepid explorer. The FA and IP thresholds, or equivalent parameters depending on the precise DTT algorithm employed, are selected by the operator in an effort to insure that the tracking process will cease when minimal anisotropy or insufficient correlation of directions between neighboring voxels is observed, typically in grey matter or CSF regions. An excellent example of determining optimal FA and IP values for axonal tracking in the brainstem can be found in the work by Stieltjes et al. [31] who used the fiber assignment by continual tracking methodology. Intrarater and interrater variability for identifying five major tracts in the brainstem were minimized when FA and IP lower cutoff values around 0.25 and 0.75, respectively, were set as thresholds [31]. Of course, acquisition details such as image plane (preferably selected orthogonal to major tracts of interest), spatial resolution (isotropic vs. anisotropic voxels) and signal-to-noise ratio will all affect the performance of any given tracking

¹ Though literary references abound for this nomenclature, our inspiration arises from Joni Mitchell's work “Don Juan's Reckless Daughter.”

algorithm. In its present form, however, DTT appears to bear up well with qualitative comparisons of what is known regarding white matter fiber tract anatomy. It has become fairly well accepted that DTT may be used to identify major fiber tracts and also to measure aspects such as D_{ave} and FA along such tracts. One must be aware, however, of the computational difficulties and operator-dependent nature of the resulting DTT maps and computed parameters. Even in its present, semiquantitative form, however, DTT is being used in conjunction with fMRI studies to locate and assess connectivity between functional areas of the cortex, a subject we review following a brief description of basic fMRI methodology.

3. Functional magnetic resonance imaging

At first sight, the term *functional magnetic resonance imaging*, or fMRI, might appear to be a very general term not referring to any specific organ in particular. For example, muscle function during exercise might be assessed through the rate of phosphocreatine depletion, as monitored with ^{31}P MRI. Liver function might be assessed by Kupffer cell uptake of specially designed MRI contrast agents. Although clearly such types of studies fall under the general subject category of fMRI, it would be a brave soul indeed who would glibly refer to such studies as fMRI. No, the term *fMRI* has effectively been confiscated by practitioners interested in how the brain works — and, with over 40,000 “fMRI” papers in the literature since its inception some 15 years ago [36], there appears to be no turning back. So we turn to a brief, basic description of what is generically meant by fMRI as related to determining the areas of our brains, which “activate” or “function” as a consequence of the various mental and physical tasks that make up our lives.

Gray matter, rich in neuronal cell bodies, is the primary tissue associated with functional activation. As known long before fMRI, specific regions of gray matter are associated with specific tasks such as finger tapping, foot movement, visual stimulation, cognitive processes, etc. These activated regions demonstrate a hemodynamic response, which can be detected with suitable MRI methods. Although many of the details responsible for the signal change accompanying the hemodynamic response remain under investigation [37], there is general agreement that increased levels of oxygenated blood, with subsequently decreased levels of paramagnetic deoxyhemoglobin molecules, are responsible for the observed signal change. The decreased level of deoxyhemoglobin results in reduced spin dephasing and a subsequently longer transverse relaxation time $T_2^* = 1/R_2^*$, where R_2^* is the transverse relaxation rate per second. In the simplest model, the increase in oxygenated blood at the activated site results in a reduction of R_2^* by a small increment ΔR_2^* . As a result, the T_2^* weighting of an image acquired with an echo time T_E in the activated state is $\exp(-T_E(R_2^* - \Delta R_2^*))$ while the weighting for the unactivated state is $\exp(-T_E R_2^*)$. The difference between the

signals in the activated vs the unactivated state ΔS , to first order in $T_E \Delta R_2^*$, may thus be written as

$$\Delta S = [p(1 - \exp(-T_R/T_1))]T_E \Delta R_2^* \exp(-T_E R_2^*). \quad (6)$$

Here, the term in brackets is the standard longitudinal relaxation time (T_1) dependence, with T_R being the repetition time; spin density (p) weighting and changes in these two parameters have been assumed negligible between activated and unactivated states. Note that the function described by Eq. (6) has a maximum at $T_E = 1/R_2^* = T_2^*$. This is why it is common practice to employ EPI sequences with T_E values set between 45 and 75 ms for fMRI studies, as this is the approximate range of T_2^* values for brain parenchyma [38,39].

The majority of fMRI studies utilize the simple change in signal embodied by Eq. (6) to locate those regions of the brain that demonstrate a hemodynamic response due to “activation.” The effect is often referred to as the BOLD effect, and the most common procedure is to scan the brain quickly with EPI sequences, acquiring, e.g., 20 slices every 2.5 s. This is repeated for several minutes while, e.g., 30-s periods of activity (visual stimuli, finger tapping, etc) are followed by 30-s periods of nonactivity, and so on. The entire fMRI data sets are then analyzed for statistical differences between the “on” and “off” states using any number of software packages now available, such as the statistical parameter mapping (SPM99) package (<http://www.fil.ion.ucl.ac.uk/spm/spm99.html>) based on the linear model of Friston et al. [40]. Although the “on-off” strategy, or “blocked task paradigm,” for stimuli presentation is most common, other strategies for stimuli presentation such as “event-related” responses [41,42] may be more appropriate for some types of cognitive tasks. In general, the mode of stimuli presentation should be considered carefully when planning an fMRI study.

This brief description of the basic fMRI experiment, as elucidated many years ago by several groups [43–47], must be supplemented considerably for a full appreciation of the technique and its limitations. Spatial resolution limitations and, even more critically, the complexity of the BOLD-induced signal changes often make unambiguous localization of the truly activated areas problematic. For example, signal changes from regions around veins that drain activated areas can distort and magnify the shape and size of the actual activated regions, a subject largely beyond the scope of the present work but one which should be appreciated when performing fMRI studies and choosing appropriate acquisition strategies [47–50].

4. Combining fMRI and DTT; a homegrown example

Figs. 1–3 show data from our laboratory in which DTI data sets have been used to generate limited tractography maps starting from seed regions defined by fMRI-based activation of the motor and the visual systems. All data was acquired with a 3T scanner (General Electric Medical

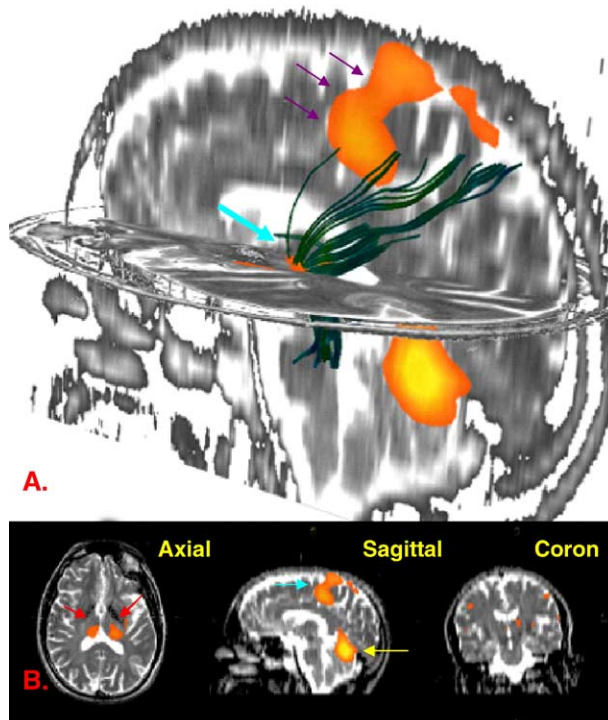


Fig. 1. Rendering of adult brain in which left hemisphere motor fiber tractography and fMRI activation map for the contrast, finger tapping vs. rest, are superimposed on the same subject's anatomic image. (A) Motor tract fibers in green emanate from region of fMRI motor cortex activation (orange region indicated by purple arrows and used as the seed region) and travel toward subcortical gray matter (indicated by aqua arrow). (B) fMRI results in all three planes. In the axial view, bilateral subcortical grey matter activation is seen (red arrows) while motor cortex and midline cerebellar activations are seen on sagittal view (aqua and yellow arrows, respectively).

Systems, Milwaukee, WI, USA) in one single session using a 48-year-old male subject. The DTI data were acquired with a Line Scan Diffusion Imaging sequence [51], while the fMRI data were acquired using standard EPI gradient echo sequences with 30-s on-off paradigms with checkerboard stimulation for visual activation and bimanual tapping for motor activation. The tractography algorithm was implemented as part of the 3D Slicer package of the Surgical Planning Laboratory at the Brigham and Women's Hospital and used an FA cutoff value of 0.1. Activation maps were obtained using standard SPM software (<http://www.fil.ion.ucl.ac.uk/spm/spm99.html>).

Fig. 1A presents an amalgamate of the DTT and the fMRI study of the motor system, with activation areas identified from the bimanual tapping paradigm. In Fig. 1A, the left hemisphere motor fiber tractography and fMRI activation areas found from the finger tapping versus rest periods are superimposed onto the subject's T2-weighted anatomic images. The motor tract fibers in green emanate from a region of fMRI motor cortex activation (orange region indicated by purple arrows and used as the tractography seeding region) and travel toward subcortical gray matter (indicated by aqua arrow). Fig. 1B shows the fMRI results of the same subject in all three planes. In the

axial view, bilateral subcortical grey matter activation is seen (red arrows) while motor cortex and midline cerebellar activations are seen on the sagittal view (aqua and yellow arrows, respectively).

Fig. 2 shows left hemisphere optic radiation tracts and the fMRI visual activation map obtained by reverse checkerboard flash superimposed on the subject's anatomic T2-weighted image. Optic radiation fibers are seen in green to emanate from a region of fMRI activation (orange region indicated by aqua arrow and used as seed region) in left lateral geniculate nucleus of thalamus and travel toward striate cortex in occipital lobe (indicated by purple arrows). Fig. 3 shows the DTI tractography and fMRI visual activation map superimposed upon the subject's anatomic images demonstrating white matter fibers that traverse the posterior corpus callosum and connect areas of activated visual cortex in each hemisphere. In Fig. 3A, a seed point in the left occipital cortex within an area of visual activation was used to propagate fiber tracts (see aqua arrows pointing to green fibers). Fibers traverse the sagittal slice and appear on the opposite side of the sagittal slice in Fig. 3B, where the same fiber tract seen in Fig. 3A is viewed from the opposite side of the sagittal slice. Fibers sweep forward and upward (aqua arrows) to cross in the region of the posterior corpus callosum (magenta arrow). In Fig. 3C, transcallosal fibers seen in B emerge in right hemisphere (green arrow) and sweep posterior to ramify in right occipital cortex that demonstrates fMRI activation to visual stimulation (purple arrow; note that sagittal slice presented is now located in the right hemisphere). The origin of fiber tract derived from the seed point in occipital cortex in the left hemisphere presented in Fig. 3A is indicated by the aqua arrow.

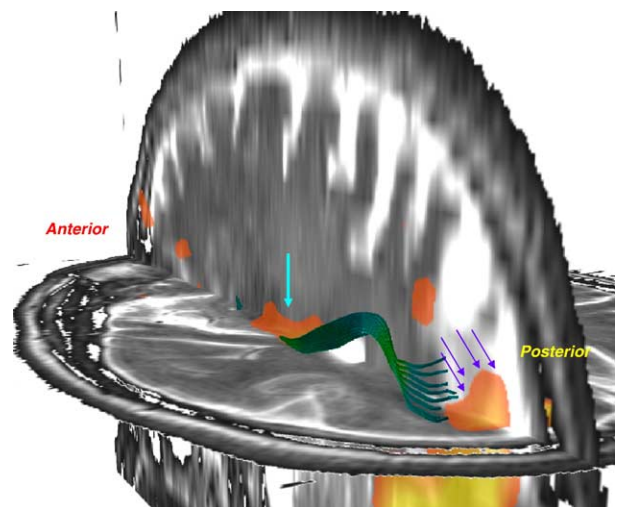


Fig. 2. Rendering of adult brain in which left hemisphere optic radiation tractography and fMRI visual activation map by reverse checkerboard flash are superimposed on the same subject's anatomic image. Optic radiation fibers are seen in green to emanate from region of fMRI activation (orange region indicated by aqua arrow) in left lateral geniculate nucleus of thalamus and travel toward striate cortex in occipital lobe (indicated by purple arrows).

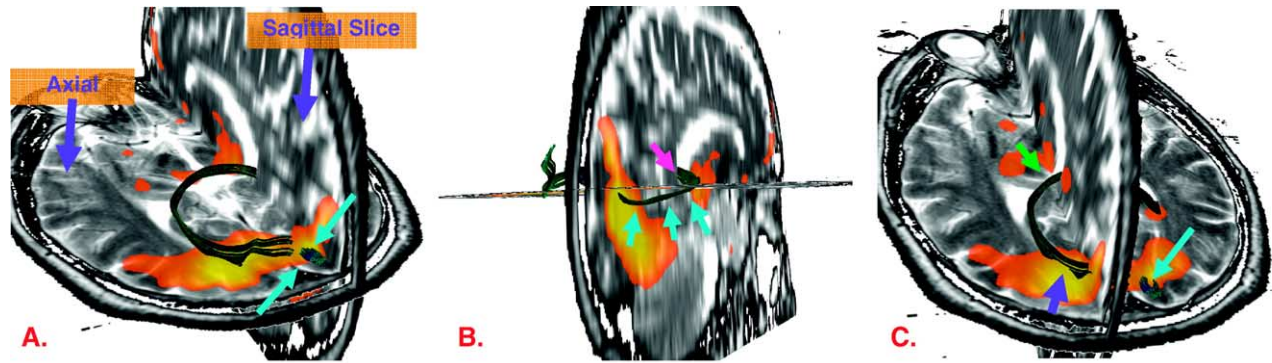


Fig. 3. DTI tractography and fMRI activation map for visual activation superimposed upon the subject's anatomic images demonstrating white matter fibers that traverse the posterior corpus callosum and connect areas of activated visual cortex in each hemisphere. (A) A seed point in the left occipital cortex within an area of visual activation is used to propagate fiber tracts (see aqua arrows pointing to green fibers). Fibers traverse the sagittal slice and appear on the opposite side of the sagittal slice in B. (B) Same fiber tract as seen in (A) but viewed from the opposite side of the sagittal slice. Fibers sweep forward and upward (aqua arrows) to cross in the region of the posterior corpus callosum (magenta arrow). (C) Transcallosal fibers seen in (B) emerge in right hemisphere (green arrow) and sweep posterior to ramify in right occipital cortex that demonstrates fMRI activation to visual stimulation (purple arrow; note that sagittal slice presented is now located in the right hemisphere). Origin of fiber tract derived from the seed point in occipital cortex in the left hemisphere presented in (A) is indicated by the aqua arrow.

These examples we have provided are representative of the capabilities of many current research laboratories and demonstrate how structure and function in the human brain can be accessed together using combined DTI and fMRI studies. We now turn to an overall review of the available literature in which the structural aspects of diffusion imaging, primarily for white matter, are complemented by functional studies of activation, primarily in gray matter. Though relatively new, this intriguing field is maturing, and there is now a reasonable body of literature from which an appreciation of the complementary aspects of diffusion imaging and fMRI for studying structure and function begins to emerge.

5. Visual system

Werring et al. [52] were among the first to demonstrate complementary aspects of DTI and fMRI in the visual system of healthy humans. They point out that both DTI and fMRI usually use single-shot echo planar imaging (EPI) sequences in which spatial distortions are common due to the necessarily long readouts in the presence of susceptibility and/or chemical shift effects. This is generally accepted as a disadvantage when probability distributions representing activation maps or DTI-derived quantities are overlaid on undistorted structural images for visualization purposes. What Werring et al. emphasized is that if three primary EPI acquisition parameters for the DTI and fMRI scans — the receiver bandwidth, echo spacing and number of echoes — are matched, then the spatial distortions caused by off-resonance effects (tissue susceptibility differences, chemical shift, etc) will be practically identical. This then allows for direct overlays of fMRI activation maps with DTI-derived maps without worrying about the sophisticated corrections for the spatial distortions often employed when either modality is used individually with high-resolution, undis-

torted anatomical images. Their primary finding, however, was that the voxels within the visual cortex, which were activated by 8-Hz flash photic stimuli, were associated with smaller FA values than neighboring optic radiation white matter. Specifically, mean FA values of 0.40 ± 0.14 were reported in activated voxels ($n=5$ subjects) compared to mean FA values of 0.69 ± 0.03 in unactivated optic radiation white matter. The finding was attributed to the fact that the activation primarily occurs in neuronal cell bodies of grey matter within which water molecules do not experience the highly structured environment found within the fiber tracts of white matter [52].

Conturo et al. extended the work of DTI and fMRI in the visual system by including not just the standard DTI data of intravoxel eigenvector directions and FA but also the intervoxel information contained in tractography analyses of DTI data [28]. As discussed above, tractography generally involves selection of seed points to initiate the fiber tracking algorithm, which then proceeds to generate connected fiber tracts. Conturo et al. selected their seed points within activating regions of the visual cortex, as identified from the fMRI data. With this approach, they succeeded in demonstrating the geniculocalcarine fiber tracks connecting the thalamus to the visual cortex. The groups of diffusion tracks generated were, overall, consistent with known anatomy, although some unanticipated results with fiber tracts segregating within the outer layers of the splenium were also reported. In this study, the combination of tractography methods with activated areas identified from fMRI required the use of a “border filtration” approach in which the boundaries of the activated regions were extended somewhat beyond their natural borders. The step was necessary to allow for the fact that the tractography algorithm employed required an operator-defined threshold FA value in order to find and extend the fiber locations. As discussed by Werring et al. [52], within activated regions,

the FA values may be quite low and, so, fall below this threshold value due to the association with grey matter, thus requiring the border filtration approach employed by Conturo et al. [28].

More recently, Toosy et al. [53] applied the combined tractography/fMRI approach to quantify and correlate relations between the degree of activation within the visual cortex and the mean FA values associated with the optic radiations emanating from and/or towards them. They employed the Probabilistic Index of Connectivity (PICO) tractography algorithm [32,33], in which a probability between 0 and 1 is assigned to each voxel, which represents the probability that that particular voxel is connected to the seed voxel. In this case, different fiber tractographic maps were generated using different cutoff values for the probability assignment, with the general finding that higher cutoff values were associated with smaller volumes of optic radiations, the fibers of which demonstrated higher mean FA values. For the fMRI studies, monocular photic stimulation to each eye was employed, although in the final analyses, responses from both eyes were averaged. Two measures of fMRI activity were generated using SPM software and structural normalization to the stereotactic space defined by the Montreal Neurological Institute standard. The spatial extent of the activated region was quantitatively estimated using a count of the number of voxels, the signal intensity changes of which exceeded a specific threshold, a quantity which the authors referred to as fMRIvox. In addition, another fMRI parameter associated with the degree or strength of the contrast attained between activated and unactivated states among the activated voxels, called fMRIPE, was extracted from the analysis. These measurements were made from a 2-cm spherical region encompassing the posterior visual cortex.

The important finding was a positive correlation between both fMRIvox and fMRIPE and the mean FA value of the optic radiations regardless of the PICO cutoff criterion. The quantitative analyses employed and the striking correlations observed led the authors to make the persuasive suggestion that visual cortex response is “constrained” by the integrity of the subservient connections, in this case, the optic radii. Intriguingly, the tractography results also demonstrated significantly larger optical tracts in the female subjects ($n=7$) vs the male subjects ($n=15$). This finding was noted to be consistent with results from Good et al. [54] who utilized high resolution T1-weighted images and morphometric analyses to assess white matter volumes associated with optic radiations.

Before moving beyond studies involving the visual system, two additional works combining DTI, tractography and fMRI to help identify and study the structure–function relationship should be noted [55,56]. In the first, high-field (9.4 T) data from cat brain *in vivo* were acquired with standard DTI and fMRI methods [55]. The use of high field strengths allows for high spatial resolution and high signal-to-noise data to be acquired from small animals, and the

resulting fiber tractography maps, obtained using seed points within the visually activated areas of the cat brain, are quite spectacular. In particular, by using the fMRI visually activated areas 17 and 18 and the lateral geniculate nucleus (LGN) as seed points for the fiber tracking algorithm, with an FA threshold of 0.2, the white matter axonal circuitry linking the primary visual areas with the LGN was completely elucidated. The article nicely demonstrates how bringing to bear the full apparatus of fMRI, DTI and tracking algorithms can allow for assessing neuroanatomical connections between activated areas in small animals, which can then, of course, be used for validating the techniques with follow-up histology. The second study of note [56] broaches a topic that we will explore in greater detail in a future review: how diffusion weighting of fMRI acquisitions influences the size, shape and degree of activation. Song et al. [56] have demonstrated this effect nicely in the visual system of six healthy subjects by incorporating dynamically changing b factors of 2, 166 and 230 s/mm^2 into fMRI runs of photic stimulation. By acquiring 210 time points during 3.5 min of 30-s on–off periods, separate analyses of the BOLD changes from 70 images each for the different b factor weightings become available. The primary finding is that the areas of activation recovered from the low b -factor setting, which largely corresponds to standard fMRI data but, with some arterial signal loss, are larger and more overlapping than the smaller distinct areas of activation recovered at the higher b -value settings. The latter areas proved much more reliable for establishing the seed regions from which tractography could proceed and map out fiber connections between primary (V1), secondary (V2) and middle temporal areas [56]. The nature of the BOLD signal is still under study and the article by Song et al. [56] demonstrates how the incorporation of diffusion weighting into fMRI acquisitions should add significantly to a better understanding of the underlying mechanisms contributing to the BOLD signal.

6. Motor system

Guye et al. [57] studied the primary motor cortex (M1) system structure/function relationship in eight healthy, right-handed males ranging in age from 20 to 46 years and also in one right-handed 30-year-old male subject with a left frontal lesion resulting in frontal lobe epilepsy. As suggested by Werring et al. [52], they performed the DTI and fMRI acquisitions with EPI readouts with identical bandwidth, field of view and matrix size so that geometric distortions, while not eliminated, were essentially the same for both acquisitions and, so, allowed for highly correlated spatial registration between the two types of data. This, in turn, permitted the use of FA maps to select three seed points in the white matter immediately adjacent to the M1 area activated by the simple left and right alternating hand-tapping paradigm used for the fMRI motor task. Fiber

connectivity maps were generated using all three seed points near M1 with the fast marching tractography algorithm, [32,33] excluding voxels with FA values lower than 0.1. This setting of the FA threshold was stated to avoid artifactual pathways through CSF while allowing for corticocortical fiber connections to proceed. The final connectivity maps, in which values between 0 and 1 represent the probability of connection between a given voxel and a seed voxel, were generated as “union maps” in which the connectivity value retained for any given voxel was the maximal connectivity value from each of the three different maps generated from the three distinct seed voxels. A rationale for the use of union maps vs maps generated from the mean of the three separate maps was provided, in which union maps were stated to avoid overlaps between the three connectivity maps while providing high-connectivity values to subsampling sections of the maps with high connectivity.

Three groups of fiber tracts were identified on the basis of their range of connectivity values. In the high connectivity range (>0.3), at least nine groups were identified, including a group which followed the pyramidal tracts and groups associated with premotor areas such as superior frontal gyrus and supplementary motor area. Other groups in the high connectivity category included tracts associated with the parietal lobe and a group which followed the corticospinal tract and which involved portions of the thalamus, although spatial resolution limits precluded definitive identification of the nuclei involved. Groups of tracts with more moderate values of connectivity between 0.2 and 0.3 were observed associated with corticospinal tracts, thalamus, corpus callosum and cerebellar peduncle. Regions of the brain in which connectivity values were less than 0.2 were nonspecific to the motor system. In this right-handed group of healthy control subjects, M1 connectivity was more extensive in the dominant left hemisphere. For example, a group of tracts involving the superior part of the left occipital lobe and another group associated with the left superior temporal gyrus and the left occipitotemporal junction were not observed in the right hemisphere. The left hemisphere, overall, had higher connectivity values than the right with only two areas of higher connectivity observed on the right, these being white matter below the precentral gyrus in the corona radiata and white matter of the lateral premotor cortices. The one patient examined in this study who had the left medial precentral lesion demonstrated displaced connections to the supplementary motor area within the left hemisphere. Also, on the left, the patient had premotor and posterior parietal lobe connectivity values somewhat higher than those found in the averaged controls but lower connectivity values in the corticospinal tracts than those found in the controls. This latter finding was treated as possibly artifactual due to pathological modifications leading to increased partial volume effects, since the patient had no motor deficit. Some connectivity differences from controls were also found in the right hemisphere despite the lack of any lesion in this hemisphere.

7. Development of working memory

Olesen et al. studied the correlation between the gray and white matter maturation occurring in mid- to late adolescence, which is thought to be associated with cognitive capacities of working memory [58]. A previous fMRI study from this group [59] had demonstrated increased gray matter activity in frontal and parietal regions as working memory capabilities developed during childhood. The group hypothesized that the increased activity observed might be reflected in maturation of associated white matter and tested this hypothesis using combined fMRI studies of working memory, with DTI measures of white matter maturation in 23 healthy, right-handed children (9 females and 14 males) ranging in age from 7.8 to 18.5 years. The authors point to studies in which myelination and neural activity have been shown to be related and, in particular, how the speed of neural transmission is related to axon diameter and the thickness of the myelin sheets [60]. The latter two physical attributes of fiber anatomy are known to affect the DTI-derived FA values and, so, correlations were sought between increased fMRI activity in gray matter associated with working memory tasks and with FA values extracted from DTI analyses of white matter in specific regions associated with working memory circuitry. Independent assessments of working memory outside of the scanner were also performed to determine brain regions where FA and/or BOLD responses correlated with the comprehensive working memory scores.

Results from the study revealed four regions where FA correlated with working memory, primarily in the left hemisphere in these right handed subjects; the frontoparietal white matter, anterior corpus callosum (left and right frontal lobes), anterior frontal white matter and left temporo-occipital white matter. The regions identified from fMRI of working memory tasks that correlated with the comprehensive working memory score were only in the left hemisphere and consisted of the head of the caudate nucleus, superior frontal sulcus and the inferior parietal lobe. From the “in-scanner” data alone, a fairly impressive, positive correlation was found between the BOLD response in the superior frontal sulcus and the mean FA values measured in the superior frontal sulcus. Other correlations were also found between the activity in the head of the caudate nucleus and the FA values in the anterior corpus callosum and in the temporo-occipital white matter. These results, similar in kind to those reported by Toosy et al. [53] for the visual system, demonstrate how cortical activity from even cognitive tasks like working memory are constrained by the maturity/integrity of the supporting white matter fiber tract connections, as reflected by the DTI-derived FA values. Fiber tracking per se was not performed as part of this study, and it remains unclear whether using tractographic rather than anatomically defined region-of-interest analyses would have improved the correlations.

8. Pathologies

To date, a number of pathological conditions such as multiple sclerosis [61], migraine [62], and patients with brain lesions causing specific neurological sequelae [63–65] have been studied with the structure/function complementarity of diffusion imaging and fMRI, as now reviewed.

Filippi et al. combined fMRI studies of motor activation with DTI studies of white matter integrity in a group of primary progressive multiple sclerosis (PPMS) patients with age- and sex-matched controls [61]. They hypothesized that cortical reorganization, as reflected by the fMRI differences between PPMS and control subjects, might be a response to the early white matter tissue damage as observed with lesion load from standard MRIs as well as with the more subtle tissue damage detected in normal-appearing brain tissue (NABT) with DTI or magnetization transfer (MT) studies. A four-finger flexion–extension test used for the fMRI activation study revealed the standard contralateral hemisphere activation in the control subjects, while the PPMS patients showed greater activation bilaterally. Furthermore, the bilateral activation of the supplementary motor area (SMA) in PPMS patients showed moderate correlations ($r=0.62$ and $r=-0.65$), with the mean diffusion coefficient and the peak height associated with the NABT diffusion histogram generated from brain tissue with T2 lesions specifically excluded. The mean diffusion coefficient in NABT was approximately 4% higher in PPMS patients, with the difference being statistically significant, while the mean peak height of the diffusion histogram was reduced in PPMS patient by a statistically significant amount (~15%) compared to controls. The authors interpret the peak height of diffusion histograms from NABT as a measure of the “residual amount of truly normal tissue” [62] so that observed reductions in this peak height indicate that even NABT is compromised by the disease. The average lesion diffusion coefficients were not correlated with the degree of fMRI activation. Fractional anisotropy measures were not reported despite the use of a DTI acquisition protocol, which involved diffusion sensitization along eight noncollinear directions. The authors suggest that the cortical reorganization observed in the fMRI studies, which correlated with structural DTI related parameters within the “normal” parts of the brain, may help “limit the consequences of MS injury in the brain. . .”

A similar study was performed by the same group in which results from fMRI motor activation and DTI examinations were compared between 15 right-handed patients with migraine headaches and 15 age- and sex-matched right-handed control subjects [62]. Standard headache classification for migraine and the existence of at least four brain MRI abnormalities were inclusion criteria for the migraine population. All subjects had a normal neurological examination. As with the PPMS study, the migraine patients showed a statistically significant diminished peak height (~9%) for the diffusion histogram of the

normal-appearing white matter compared to controls, although the mean diffusion coefficients were similar in both groups. Activation patterns were somewhat different between the two groups with the migraine patients showing (a) greater activation of the contralateral primary sensorimotor cortex and (b) a displacement of the center of the activated cluster rostrally of the SMA in the migraine patients. The latter finding was attributed to greater activation of the pre-SMA, located more rostrally than the more caudal SMA proper, possibly due to patient perception of the task as relatively difficult compared to control subjects. An intriguing negative correlation between the relative activation of the SMA and the diffusion histogram peak height was also reported, supporting the authors’ suggestion that widespread white matter damage may cause greater motor activation observed in the fMRI studies of the migraine patients [62].

Among the studies of individual patients with interesting brain lesions causing specific neurological deficits is that of Molko et al. [63] who performed DTI, including tractography, and a visual/word form activation fMRI study in a patient with lesion-related alexia in his left visual field. The fMRI studies focused on visually coactivated regions in the left- or right-hemisphere retinotopic areas and the so-called verbal word form area (VWFA). The latter is thought to be located in most individuals in the left inferior occipitotemporal region. Evidence suggests that word presentation in a single hemifield of vision, left or right, activates contralateral retinotopic areas and then consistently activates the VWFA [64]. Molko et al. found, indeed, that VWFA coactivated with either the left or right retinotopic areas as words were presented within the right or left half field of vision, respectively, in normal subjects. In a patient with division of the posterior half of the corpus callosum due to prior surgery, however, only a very weak activation of VWFA was observed when words were presented within the left half of the visual field despite normal activation of the right retinotopic area. The findings are consistent with damage to fiber tracts connecting the right retinotopic area with the VWFA located in the left hemisphere. The DTI data, indeed, revealed damaged fiber tract connections between the left and right ventral occipitotemporal regions, yielding FA values some two to three times smaller than corresponding FA values measured within the control group. Damaged fiber tracts were not only observed directly in the lesion within the corpus callosum, a lesion readily identified from even T1-weighted images, but also within regions outside of the obvious lesion and along the primary tracts connecting the left-hemisphere VWFA with the right retinotopic visual activation region. The authors introduced a “negative tracking” concept for visualizing the damaged fiber bundles, which was based on identifying voxels with statistically significant reductions in FA and were able to nicely depict postulated pathways of the damaged transcallosal tracts [63].

Another remarkable combination fMRI/DTI study was reported by Werring et al. [65] on a 21-year-old male subject who sustained an injury from a snooker cue² through his right orbit, penetrating through the right frontal lobe to the right parietal cortex. A strong left hemiplegia was the immediate aftermath, though this largely resolved over a month. When the scans were performed 18 months later, only some residual motor symptoms were apparent, among them, a slow gait, dystonic posturing of the left foot and left hand fatigue. The goal of performing both fMRI and DTI together in this subject was stated to be an effort to “...investigate mechanisms of recovery and persistent deficit in an individual patient.” Recovery was attributed to reversible features of the injury, such as edema resolution and reduction of mass effects, and/or to reorganization of cortical pathways to compensate for damage to the motor system. The fMRI studies were performed using unilateral finger tapping alternated with rest periods, and the standard contralateral activation responses in the primary motor cortex and supplementary motor cortex were observed. There was however, some ipsilateral activation in the primary motor cortex observed for left hand finger tapping, suggesting some reorganization in response to the injury. From the DTI data, FA maps at the level of the injury showed the structural damage nicely at 18 months. These maps clearly showed that portions of the internal capsule, primarily anteriorly, were most affected by the injury. The FA values in the anterior limb of the right internal capsule were reported to be 0.29 ± 0.14 , compared to FA values around 0.75 observed in control subjects ($n=5$). The posterior limb of the right internal capsule was spared, demonstrating a near-normal FA value of 0.72. The authors suggest that the latter fiber tracts are more “clinically important” for limb control than those located anteriorly, and so, despite the irreversible nature of the loss of fiber tract integrity anteriorly, near-full recovery was observed in this patient. A noted limitation of the study was the relatively long interval between injury and fMRI/DTI information, 18 months in this case. They suggest that earlier studies and studies performed longitudinally would be more informative as to whether early recovery might be attributed to more widespread cortical reorganization that subsides once the reversible damage had been repaired. The study certainly shows the potential of combined fMRI and diffusion imaging to sort out mechanisms of repair from serious injury on an individual patient basis.

Finally, Henry et al. [66] performed an interesting DTT study of the connections between regions of the brain associated with motor speech and naming but without the use of fMRI. Rather, the seed points for the specific language tasks were chosen from direct cortical stimulation as performed intraoperatively in a brain tumor patient. This direct approach allowed the investigators to identify eight

specific regions on the cortex corresponding to sites of jaw and mouth stimulation as well as speech arrest and anomia — the inability to name an object despite being capable of speech. Fiber tracks generated from seed points in the stimulation sites were in general agreement with known fiber tract anatomy, with subcortical connections to the pyramidal tract and the supplementary motor area, a region known to result in speech arrest and/or anomia when stimulated [67]. The authors point out that although fMRI and magnetic source imaging are both potential candidates for preoperative identification of eloquent cortex, intraoperative cortical stimulation remains the gold standard. As such, direct cortical stimulation is, as suggested, an interesting approach for validating diffusion tensor tractographic methods as they continue to mature.

9. Conclusions

The advent of diffusion imaging and fMRI, as part of the standard tools of modern MRI scanners, opens up new possibilities for studying the interplay between structure and function in the human brain. Significant progress has been made already in this area by combining the two modalities, particularly for the visual and motor systems. The combined use of diffusion imaging and fMRI provides a synergy, which will expand the utility of each beyond the more specialized applications associated with each methodology alone and will further our basic understanding of how the brain works.

Acknowledgments

The authors would like to thank Dr Bruno Maraviglia and his colleagues at the University of Rome who graciously sponsored and organized the productive 2005 school/workshop on brain structure and function in Erice, Sicily, for which this review was prepared.

References

- [1] Gonzalez RG, Schaefer PW, Buonanno FS, Schwamm LH, Budzik RF, Rordorf G, et al. Diffusion-weighted MR imaging: diagnostic accuracy in patients imaged within 6 hours of stroke symptom onset. *Radiology* 1999;210:155–62.
- [2] Beauchamp NJ, Bryan RN. Acute cerebral infarction: a pathophysiologic review and radiologic perspective. *AJR Am J Roentgenol* 1998;171:73–84.
- [3] Lutsep HL, Albers GW, DeCrespigny A, Kamar GN, Marks MP, Moseley ME. Clinical utility of diffusion-weighted magnetic resonance imaging in the assessment of ischemic stroke. *Ann Neurol* 1997;41:574–80.
- [4] Baird AE, Benfield A, Schlaug G, Siewert B, Lovblad K-O, Edelman RR, et al. Enlargement of human cerebral ischemic lesion volumes measured by diffusion-weighted magnetic resonance imaging. *Ann Neurol* 1997;41:581–9.
- [5] Moseley ME, Butts K, Yenari MA, Marks M, de Crespigny A. Clinical aspects of DWI. *NMR Biomed* 1995;8:387–96.
- [6] Chenevert TL, McKeever PE, Ross BD. Monitoring early response of experimental brain tumors to therapy using diffusion magnetic resonance imaging. *Clin Cancer Res* 1997;3:1457–66.

² The American equivalent would be a pool stick.

- [7] Mardor Y, Pfeffer R, Spiegelmann R, Roth Y, Maier SE, Nissim O, et al. Early detection of response to radiation therapy in patients with brain malignancies using conventional and high b-value diffusion-weighted magnetic resonance imaging. *J Clin Oncol* 2003;21:1094–100.
- [8] Callaghan PT. Principles of nuclear magnetic resonance microscopy. Oxford (UK): Clarendon Press; 1991. p. 157–72.
- [9] Le Bihan D Editor. Diffusion and perfusion magnetic resonance imaging: applications to functional MRI. New York (NY): Raven Press, Ltd.; 1995. p. 134–79.
- [10] Stejskal EO, Tanner JE. Spin diffusion measurements: spin echoes in the presence of a time-dependent field gradient. *J Chem Phys* 1965; 42:288–92.
- [11] Le Bihan D, Breton E, Lallemand D, Grenier P, Cabanis E, Lavaljeantet M. MR imaging of intravoxel incoherent motions — application to diffusion and perfusion in neurologic disorders. *Radiology* 1986;161:401–7.
- [12] Turner R, Le Bihan D. Single-shot diffusion imaging at 2.0 Tesla. *J Magn Reson* 1990;86:445–52.
- [13] Chenevert TL, Brunberg JA, Pipe JG. Anisotropic diffusion in human white matter — demonstration with MR techniques in vivo. *Radiology* 1990;177:401–5.
- [14] Moseley ME, Cohen Y, Kucharczyk J, Mintorovitch J, Asgari HS, Wendland MF, et al. Diffusion-weighted MR imaging of anisotropic water diffusion in cat central nervous system. *Radiology* 1990;176: 439–45.
- [15] Basser PJ, Mattiello J, LeBihan D. MR diffusion tensor spectroscopy and imaging. *Biophys J* 1994;66:259–67.
- [16] Pierpaoli C, Basser PJ. Toward a quantitative assessment of diffusion anisotropy. *Magn Reson Med* 1996;36:893–906.
- [17] Pierpaoli C, Jezzard P, Basser PJ, Barnett A, Di Chiro G. Diffusion tensor imaging of the human brain. *Radiology* 1996;201:637–48.
- [18] Basser PJ, Pierpaoli C. A simplified method to measure the diffusion tensor from seven MR images. *Magn Reson Med* 1998;39:928–34.
- [19] Beaulieu C, Fenrich FR, Allen PS. Multicomponent water proton transverse relaxation and T2-discriminated water diffusion in myelinated and nonmyelinated nerve. *Magn Reson Imaging* 1998;16: 1201–10.
- [20] Beaulieu C. The basis of anisotropic water diffusion in the nervous system — a technical review. *NMR Biomed* 2002;15:435–55.
- [21] Beaulieu C, Allen PS. Determinants of anisotropic water diffusion in nerves. *Magn Reson Med* 1994;31:394–400.
- [22] Neil JJ, Shiran SI, McKinstry RC, Schefft GL, Snyder AZ, Almlri CR, et al. Normal brain in human newborns: apparent diffusion coefficient and diffusion anisotropy measured by using diffusion tensor MR imaging. *Radiology* 1998;209:57–66.
- [23] Huppi PS, Maier SE, Peled S, Zientara GP, Barnes PD, Jolesz FA, et al. Microstructural development of human newborn cerebral white matter assessed in vivo by diffusion tensor magnetic resonance imaging. *Pediatr Res* 1998;44:584–90.
- [24] Takahashi M, Ono J, Harada K, Maeda M, Hackney DB. Diffusional anisotropy in cranial nerves with maturation. Quantitative evaluation by diffusion magnetic resonance imaging in rats. *Radiology* 2000;216: 881–5.
- [25] Douek P, Turner R, Pekar J, Patronas N, Le Bihan D. MR color mapping of myelin fiber orientation. *J Comput Assist Tomogr* 1991; 15:923–9.
- [26] Pajevic S, Pierpaoli C. Color schemes to represent the orientation of anisotropic tissues from diffusion tensor data: Application to white matter fiber tract mapping in the human brain. *Magn Reson Med* 1999;36:893–906.
- [27] Makris N, Worth AJ, Sorensen AG, Papadimitriou GM, Wu O, Reese TG, et al. Morphometry of in vivo human white matter association pathways with diffusion weighted magnetic resonance imaging. *Ann Neurol* 1997;42:951–62.
- [28] Conturo TE, Lori NF, Cull TS, Akbudak E, Snyder AZ, Shimony JS, et al. Tracking neuronal fiber pathways in the living human brain. *Proc Natl Acad Sci* 1999;96:10422–7.
- [29] Basser PJ, Pajevic S, Pierpaoli C, Duda J, Aldroubi A. In vivo fiber tractography using DT-MRI data. *Magn Reson Med* 2000;44: 625–32.
- [30] Mori S, Crain BJ, Chacko VP, van Zijl PC. Three-dimensional tracking of axonal projections in the brain by magnetic resonance imaging. *Ann Neurol* 1999;45:265–9.
- [31] Stieltjes B, Kaufman WE, van Zijl PCM, Fredericksen K, Pearlson GD, Solaiyappan M, et al. Diffusion tensor imaging and axonal tracking in the human brainstem. *Neuroimage* 2001;14:723–35.
- [32] Parker GJ, Stephan KR, Barker GJ, Rowe JB, MacManus DG, Wheeler-Kingshott CA, et al. Initial demonstration of in vivo tracing of axonal projections in the macaque brain and comparison with the human brain using diffusion tensor imaging and fast marching tractography. *Neuroimage* 2002;15:797–809.
- [33] Parker CJ, Wheeler-Kingshott CA, Barker GJ. Estimating distributed anatomical connectivity using fast marching methods and diffusion tensor imaging. *IEEE Trans Med Imaging* 2002;21: 505–12.
- [34] Ciccarelli O, Parker GJ, Toosy AT, Wheeler-Kingshott CA, Barker GJ, Boulby PA, et al. From diffusion tractography to quantitative white matter tract measures: a reproducibility study. *Neuroimage* 2003; 18:348–59.
- [35] Parker GJ, Haroon HA, Wheeler-Kingshott CA. A framework for a streamline-based probabilistic index of connectivity (PICO) using a structural interpretation of MRI diffusion measurements. *J Magn Reson Imaging* 2003;18:242–54.
- [36] Riederer SJ. MR imaging: its development and the recent Nobel prize. *Radiology* 2004;231:628–31.
- [37] Logothetis NK, Pauls J, Augath M, Trinath T, Oelternan A. Neurophysiological investigation of the basis of the fMRI signal. *Nature* 2001;412:150–7.
- [38] Speck O, Ernst T, Chang L. Biexponential modeling of multigradient-echo MRI data of the brain. *Magn Reson Med* 2001;45:1116–21.
- [39] Rivkin MJ, Wolraich D, Als H, McAnulty G, Butler S, Conneman N, et al. Prolong T2* values in newborn vs adult brain: Implications for fMRI studies of newborns. *Magn Reson Med* 2004;51:1287–91.
- [40] Friston KJ, Holmes AP, Poline JB, Grasby PJ, Williams SC, Frackowiak RS, et al. Analysis of fMRI time-series revisited. *Neuroimage* 1995;2:45–53.
- [41] Josephs O, Henson RNA. Event-related functional magnetic resonance imaging: modeling, inference and optimization. *Philos Trans R Soc Lond* 1999;354:1215–28.
- [42] Dale AM, Buckner RL. Selective averaging of rapidly presented individual trials using fMRI. *Hum Brain Mapp* 1997;5:329–40.
- [43] Ogawa S, Tank DW, Menon RS, Ellermann JM, Kim SG, Merkle H, et al. Intrinsic signal changes accompanying sensory stimulation: functional brain mapping using MRI. *Proc Natl Acad Sci U S A* 1992;89:5951–5.
- [44] Kwong KK, Belliveau JW, Chesler DA, Goldberg IE, Weisskoff RM, Poncelet BP, et al. Dynamic magnetic resonance imaging of human brain activity during primary sensory stimulation. *Proc Natl Acad Sci U S A* 1992;89:5675–9.
- [45] Thulborn KR, Gillen JS, McCurtain B, et al. Functional magnetic resonance imaging of the human brain. *Bull Magn Reson Med* 1996; 18:37–42.
- [46] Constable RT, McCarthy G, Allison T, Anderson AW, Gore JC. Functional brain imaging at 1.5 T using conventional gradient echo MR imaging techniques. *Magn Reson Imaging* 1993;11:451–9.
- [47] Oja JME, Gillen J, Kauppinen RA, Kraut M, van Zijl PCM. Venous blood effects in spin-echo fMRI of human brain. *Magn Reson Med* 1999;42:616–27.
- [48] Jochimsen TH, Norris DG, Mildner T, Moller HE. Quantifying the intra- and extravascular contributions to spin-echo fMRI at 3 T. *Magn Reson Med* 2004;52:724–32.
- [49] Song AW, Mao H, Muthupillai R, Haist F, Dixon WT. Segmented spin-echo pulses to increase fMRI signal: repeated intrinsic diffusional enhancement. *Magn Reson Med* 1999;42:631–5.

- [50] Song AW, Li TL. Improved spatial localization based on flow-moment-nulled and intra-voxel incoherent motion-weighted fMRI. *NMR Biomed* 2003;16:137–43.
- [51] Gudbjartsson H, Maier SE, Mulkern RV, Morocz IA, Patz S, Jolesz FA. Line scan diffusion imaging. *Magn Reson Med* 1996;36:509–18.
- [52] Werring DJ, Clark CA, Parker GJM, Miller DH, Thompson AI, Barker GJ. A direct demonstration of both structure and function in the visual system: combining diffusion tensor imaging with functional magnetic resonance imaging. *Neuroimage* 1999;9:352–61.
- [53] Toosy AT, Ciccarelli O, Parker GJM, Wheeler-Kingshott CAM, Miller AJ, Thompson AJ. Characterizing function-structure relationships in the human visual system with functional MRI and diffusion tensor imaging. *Neuroimage* 2004;21:1452–63.
- [54] Good CD, Johnsrude I, Ashburner J, Henson RN, Friston KJ, Frackowiak RS. Cerebral asymmetry and the effects of sex and handedness on brain structure: a voxel-based morphometric analysis of 465 normal adult human brains. *Neuroimage* 2001;14:685–700.
- [55] Kim DS, Kim M, Ronen I, Formisano E, Kim KH, Ugurbil K, et al. In vivo mapping of functional domains and axonal connectivity in cat visual cortex using magnetic resonance imaging. *Magn Reson Imaging* 2003;21:1131–40.
- [56] Song AW, Harshbarger T, Li TL, Kim KH, Ugurbil K, Mori S, et al. Functional activation using apparent diffusion coefficient-dependent contrast allows better spatial localization to the neuronal activity: evidence using diffusion tensor imaging and fiber tracking. *Neuroimage* 2003;20:955–61.
- [57] Guye M, Parker GJM, Symms M, Boulby P, Wheeler-Kingshott A, Salek-Haddadi A, et al. Combined functional MRI and tractography to demonstrate the connectivity of the human primary motor cortex in vivo. *Neuroimage* 2003;19:1349–60.
- [58] Olesen PJ, Nagy Z, Westerberg H, Klingberg T. Combined analysis of DTI and fMRI data reveals a joint maturation of white and grey matter in a fronto-parietal network. *Cogn Brain Res* 2003;18:48–57.
- [59] Klingberg T, Forsberg H, Westerberg H. Increased brain activity in frontal and parietal cortex underlies the development of visual-spatial working memory capacity during childhood. *J Cogn Neurosci* 2002;14:1–10.
- [60] Koester J. Functional consequences of passive membrane properties of the neuron. In: Kandel ER, Schwartz JH Editors. *Principles of Neural Science*. Amsterdam: Elsevier; 1985. p. 66–74.
- [61] Filippi M, Rocca MA, Falini A, Caputo D, Ghezzi A, Colombo B, et al. Correlations between structural CNS damage and functional MRI changes in primary progressive MS. *Neuroimage* 2002;15:537–46.
- [62] Rocca MA, Colombo B, Pagani E, Falini A, Codella M, Scotti G, et al. Evidence for cortical functional changes in patients with migraine and white matter abnormalities on conventional and diffusion tensor magnetic resonance imaging. *Stroke* 2003;34:665–70.
- [63] Molko N, Cohen L, Mangin JF, Chochon F, Lehericy S, Le Bihan D, et al. Visualizing the neural bases of a disconnection syndrome with diffusion tensor imaging. *J Cogn Neurosci* 2002;14:629–36.
- [64] Cohen L, Dehaene S, Naccache L, Lehericy S, Dehaene-Lambertz G, Henaff MA, et al. The visual word form area: spatial and temporal characterization of an initial stage of reading in normal subjects and posterior slit-brain patients. *Brain* 2000;123:291–307.
- [65] Werring DJ, Clark CA, Barker GJ, Miller DH, Parker GJM, Brammer MJ, et al. The structural and functional mechanisms of motor recovery: complementary use of diffusion tensor and functional magnetic resonance imaging in a traumatic injury of the internal capsule. *J Neurol Neurosurg Psychiatry* 1998;65:863–9.
- [66] Henry RG, Berman JI, Nagarajan SS, Mukherjee P, Berger MS. Subcortical pathways serving cortical language sites: initial experience with diffusion tensor imaging fiber tracking combined with intra-operative language mapping. *Neuroimage* 2004;21:616–22.
- [67] Ojemann G, Ojemann J, Lettich E, Berger M. Cortical language localization in left, dominant hemisphere. An electrical stimulation mapping investigation in 117 patients. *J Neurosurg* 1989;71:316–26.